RESEARCH ARTICLE

CHEMISTRY

Special Topic: Aggregation-Induced Emission

Aggregation-induced emission luminogens reveal cell cycle-dependent telomerase activity in cancer cells

Xia Wu[1], Jun Wu[1], Jun Dai[2], Biao Chen[2], Zhe Chen[2], Shixuan Wang[2], Feng Wu[1], Xiaoding Lou[1,*] and Fan Xia[1]

ABSTRACT

Telomerase acts as an important biomarker for tumor identification, and synthesizes telomeric repeats at the end of chromosome telomeres during the replicative phase of the cell cycle; thus, the expression level of telomerase changes as the cell cycle progresses. TERT mRNA expression and telomerase activity were significantly increased in over 80% of human cancers from tissue specimens. Although many efforts have been made in detecting the activity of TERT mRNA and active telomerase, the heterogeneous behavior of the cell cycle was overlooked, which might affect the accuracy of the detection results. Herein, the AIEgen-based biosensing systems of PyTPA-DNA and Silole-R were developed to detect the cellular level of TERT mRNA and telomerase in different cell cycles. As a result, the fluorescence signal of cancer cells gradually increased from G0/G1, G1/S to S phase. In contrast, both cancer cells arrested at G2/M phase and normal cells exhibited negligible fluorescence intensities. Compared to normal tissues, malignant tumor samples demonstrated a significant turn-on fluorescence signal. Furthermore, the transcriptomics profiling revealed that tumor biomarkers changed as the cell cycle progressed and biomarkers of CA9, TK1 and EGFR were more abundantly expressed at early S stage. In this vein, our study presented advanced biosensing tools for more accurate analysis of the cell-cycle-dependent activity of TERT mRNA and active telomerase in clinical tissue samples.

Keywords: cell cycle, TERT mRNA, telomerase activity, AIEgens, biomarkers

[1]Engineering Research Center of Nano-Geomaterials of Ministry of Education, Faculty of Materials Science and Chemistry, China University of Geosciences, Wuhan 430074, China and [2]Department of Obstetrics and Gynecology, Tongji Hospital, Tongji Medical College, Huazhong University of Science and Technology, Wuhan 430074, China

*Corresponding author. E-mail: louxiaoding@cug.edu.cn

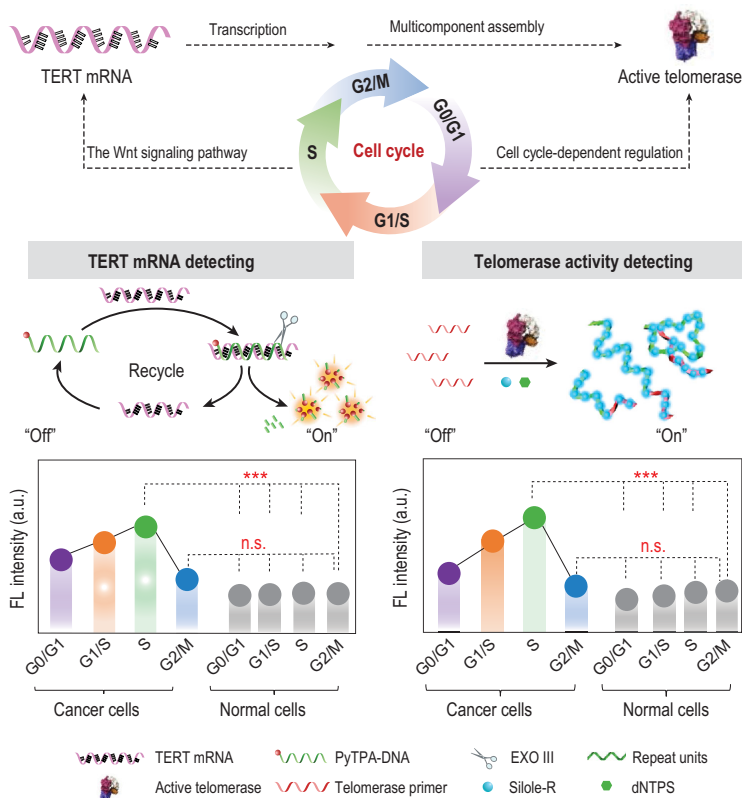## INTRODUCTION

Cancer is a significant cause of death worldwide and numerous efforts have been devoted to the development of methods for early detection and quantitative measurement of cancer biomarkers to obtain information correlated to tumorigenesis [1]. Activation of telomerase is a typical feature of more than 80% of immortalized cells but not detectable in normal somatic tissues [2,3]. Once telomerase is activated, a majority of tumor cells could maintain the telomere during the S phase of the cell cycle [4–6]. Telomerase is a ribonucleoprotein complex consisting of an RNA template moiety, a reverse transcriptase catalytic component (TERT protein) together with associated proteins [7]. Activation of telomerase is the principal manifestation of regulating the expression of TERT messenger RNA (TERT mRNA) [8,9]. In particular, telomerase activity can be inhibited by down-regulating TERT mRNA expression in different types of human malignancies [10,11]. Thus, TERT mRNA as well as telomerase activity were used as useful diagnostic biomarkers during tumorigenesis [12].

Many works have been reported in developing new bioanalytical methods for detection of TERT mRNA and telomerase activity [13,14]. Current detecting techniques (the golden standard) for TERT mRNA are mainly based on Real-time Quantitative Polymerase Chain Reaction (RT-qPCR) [15,16]. The standard TRAP assay (telomeric repeat amplification protocol) [3,17,18], optical detection [19,20], colorimetric assays [21], biosensor chip [22] and electrochemical strategies [23] have

been developed for telomerase activity detection. Fluorescence methods have the advantage of simplicity, sensitivity and rapidity [24–26], thus they were widely used in cell-lysate-dependent detecting assays [27,28] and intracellular imaging [29–31]. Moreover, our group's prior work designed a series of fluorescent probes to light up telomerase on the basis of aggregation-induced emission luminogens (AIEgens) [32–34]. AIEgens possess many advantages such as long-term tracking ability, low background and strong resistance to photo-bleaching. They exhibit a higher fluorescence in aggregated states and have been widely applied in the field of biochemical analysis and imaging [35–38].

Although lots of methods have been developed to detect telomerase, those methods mainly relied upon the analysis of asynchronous cells with different phases of the cell cycle. The cell cycle is an integrated network that contributes towards balancing the process of various bio-macromolecule syntheses, assemblies and interactions [39–41]. Some research indicates that the telomerase activity of human tumor cells changes as the cell progresses through different stages of the cell cycle [42–44]. This means

that the accurate analysis of telomerase may be affected by the different phases of the cell cycle.

Herein, we investigated the role of cell cycle progression (G0/G1, G1/S, S and G2/M phase) in analyzing telomerase (TERT mRNA and telomerase activity) in cancer cells based on an AIEgen-based fluorescence detecting system. As shown in Scheme 1, in the absence of TERT mRNA and exonuclease III (Exo III), the redundant PyTPA-DNA probe could complement hybridization and then be cleaved by Exo III to release the target and fluorogen (PyTPA-N_3). Moreover, in the presence of active telomerase, the template strand primer (TP) could be extended to form long negatively charged DNA chains. The positively charged AIE dye (Silole-R) was spontaneously combined to the chains via electrostatic interaction. On the basis of this system, we tested TERT mRNA and telomerase activity between different phases of cancer cells vs. normal cells. Results show that the fluorescence signal of cancer cells arrested at G0/G1, G1/S, S phase increased as the cell cycle progressed, while the cancer cells arrested at G2/M phase and normal cells showed a negligible intensity. Moreover, this fluorescence analyzing system was successfully used in the tissue samples of malignant tumors. Finally, we compared the expression levels of some biomarkers during difference phases of the cell cycle on the basis of transcriptomics profiling. These results, therefore, suggest that future studies on tumor biomarkers analysis, such as TERT mRNA and telomerase activity, should consider the phase of the cell cycle.

RESULTS AND DISCUSSION

Bioprobes for TERT mRNA and telomerase activity

PyTPA-N_3 was prepared according to the reported procedures [45] (Supplementary Fig. 1) and then coupled with Alk-DNA to yield PyTPA-DNA (Fig. 1A). The rude product was purified by High Performance Liquid Chromatography (HPLC) (Supplementary Fig. 1) and confirmed by High Resolution Mass Spectrometer (HRMS) with a peak at m/z 10 243.0 (Fig. 1B). The UV–Vis spectra of PyTPA-DNA exhibited a characteristic peak at 260 nm and 452 nm (Fig. 1C), respectively. The stability of PyTPA-DNA (Supplementary Fig. 2) in biological environments was confirmed. Nondenaturing polyacrylamide gel electrophoresis (PAGE) was used to demonstrate the stability of the PyTPA-DNA probes and analyze the target recycling process (Supplementary Figs 3 and 4) with assistance from Exo III. Furthermore, the mass spectrum of PyTPA-G (the hydrolysis product) was manifested
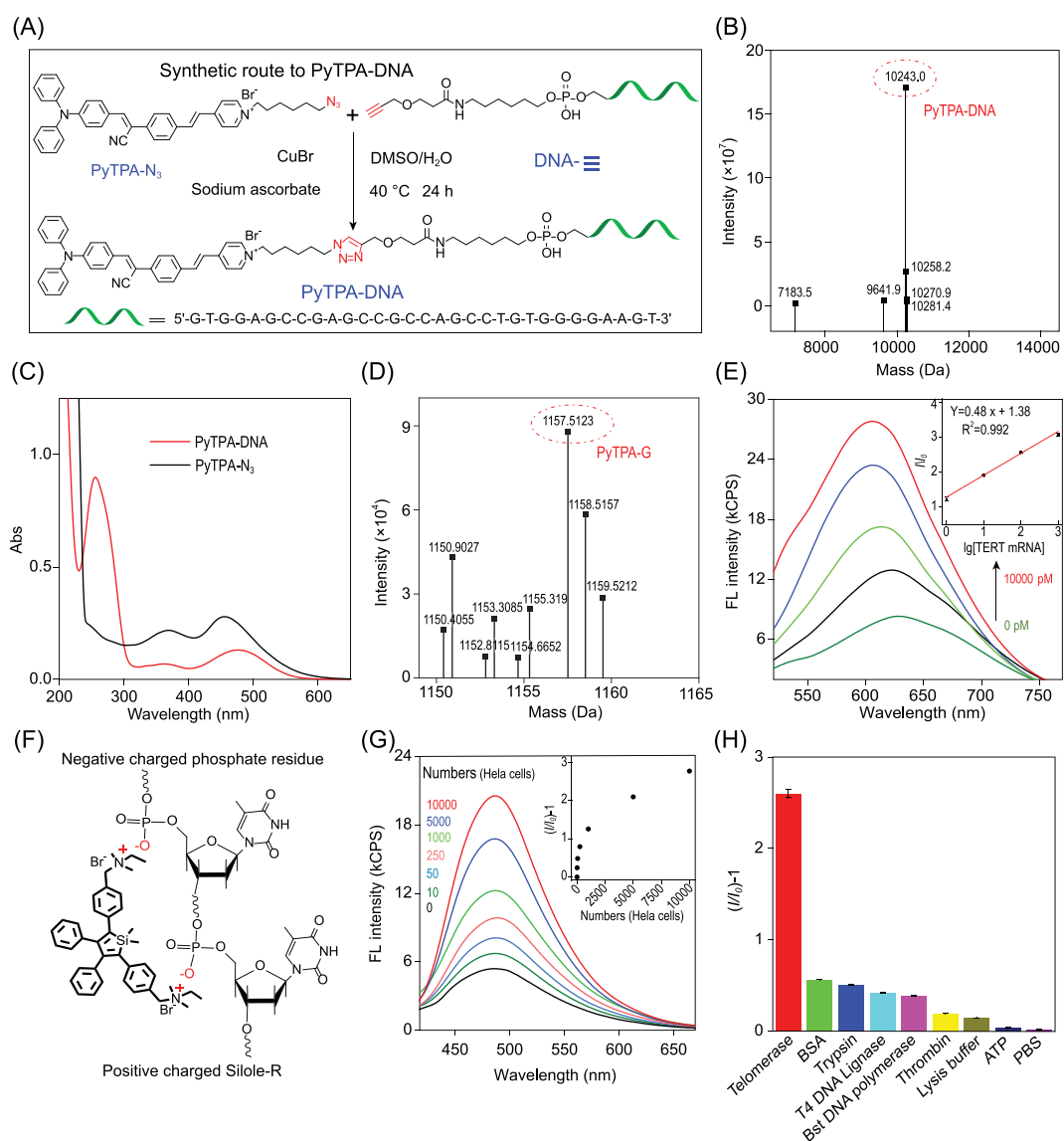

Scheme 1. AIEgen-based fluorescence detecting system for analysis of TERT mRNA and telomerase activity in different phases of the cell cycle (G0/G1, G1/S, S and G2/M phase).

(A)

(B)

(C)

(D)

(E)

(F)

(G)

(H)

Figure 1. Feasibility analysis of PyTPA-DNA and Silole-R bioprobes in analyzing TERT mRNA and telomerase activity. (A) The synthetic route of PyTPA-DNA. (B) HRMS of PyTPA-DNA. (C) The UV–Vis spectra of PyTPA-N_3 and PyTPA-DNA. (D) HRMS of the hydrolysis product PyTPA-G. (E) Fluorescence responses enhanced progressively with different concentrations of targets (0 pM, 10 pM, 100 pM, 1000 pM and 10 000 pM). (F) Electrostatic interaction between Silole-R and phosphate residues. (G) Fluorescence responses of Silole-R incubation with different concentrations of telomerase extracts. (H) Fluorescence responses (I/I_0)−1 of telomerase versus different proteins under the same experimental conditions.

at 1157.5 (Fig. 1D); the average hydrodynamic diameter of PyTPA-G was observed around 260 nm (Supplementary Fig. 5); the fluorescence intensity of PyTPA-DNA was significantly increased owing to S1 nuclease cleavage to form aggregated PyTPA-G in solution (Supplementary Fig. 6). Those results verified the successful synthesis of PyTPA-DNA and suggested that a target recycling strategy was an effective tool for detection.

On the other hand, the fluorescence intensity of PyTPA-DNA was gradually enhanced (2.9-fold) with the increased concentration of target from 0 to 10 000 pM and found to be linearly correlated with target concentrations from 10 to 10 000 pM, with detection limit of 3.36 pM ($R^2 = 0.992$) (Fig. 1E). Next, four different enzymes were used instead of Exo III in the reaction (Supplementary Fig. 7). As a result, almost no fluorescence was observed under the same treatment, suggestive of the important role of Exo III in the system. The fluorescence in response to perfectly matched strands was verified to be superior to the single/three base mismatch sequence (Supplementary Fig. 8). Finally, the fluorescence intensity of PyTPA-DNA incubated with different concentrations of RNA extracts was increased and represented reasonable correlation with

different numbers of cells (Supplementary Fig. 9). Therefore, those results confirmed the effectiveness of the PyTPA-DNA in detecting TERT-mRNA.

The synthetic route of Silole-R was reported by our literature [32,33]. Based on electrostatic force, the Silole-R was able to interact with the negatively charged DNA backbone (Fig. 1F). The fluorescence of Silole-R was weak in the solution or incubating with short single-stranded DNA (Supplementary Table 2). While, in the presence of longer sequences (Ex-6, 54-nt), a rapid fluorescence was lighted by the aggregation state of Silole-R (Supplementary Fig. 10).

The fluorescent intensities of TP and Silole-R were enhanced gradually with HeLa cells rising from 0 to 10 000, which demonstrated the positive correlation between the fluorescence emission and the cell extracts (Fig. 1G, inset). However, HeLa cells pretreated with 100 μM telomerase inhibition AZT (3′-azido-3′-deoxythymidine) exhibited no fluorescence (Supplementary Fig. 11). Only active telomerase, not other substrates, was able to initiate a potent fluorescence, suggestive of a high specificity of this bioprobe (Fig. 1H and Supplementary Fig. 12). Moreover, PAGE analysis and the TRAP method were employed to monitor the active telomerase assisted primer DNA extension, which indicated the successful elongation of DNA products with the help of telomerase (Supplementary Figs 13 and 14).

Cell-cycle-regulated TERT mRNA and telomerase activity

Four stages of HeLa cells were obtained by treatment of serum starvation, L-mimosine, thymidine and nocodazole respectively (Fig. 2A). Corresponding synchronized cell fractions were identified by flow cytometry analysis according to the DNA content (Fig. 2B and Supplementary Fig. 15).

First, PyTPA-DNA and Silole-R bioprobe were used to investigate the expression of TERT mRNA and telomerase activity under different cell cycles of HeLa cells. Figure 2C compares the fluorescence intensities (Supplementary Fig. 16) in different cell cycles. Upon progression through the cell cycle, the PyTPA-DNA faintly fluoresced in the G0/G1 stage but demonstrated an enhancement of fluorescence in response to the G1/S phase, and finally reached the strongest output in S stage. However, cells arrested at the G2/M phase showed the weakest fluorescence in contrast to the other three cell cycles. Furthermore, cell-cycle-dependent alterations of TERT mRNA expression in HeLa cells were reconfirmed by qPCR (Fig. 2D). The similar fluorescence responses of Silole-R lighted by active telomerase during different cell cycles were also received (Fig. 2E and Supplementary Fig. 17). Moreover, TRAP assay was selectively analyzed and found to have the strongest expression levels in S stage (Fig. 2F and Supplementary Fig. 18). Those detecting results revealed that the TERT mRNA amount and telomerase activity from different cancer cell cycle extracts were cell cycle dependent.

Second, the intracellular imaging of TERT mRNA and telomerase activity during different stages of cancer cell cycle were carried out. With minimal cytotoxicity of PyTPA-DNA and Exo III toward cells (Supplementary Fig. 19), PyTPA-DNA lit up HeLa cells by distributing in the cytoplasm and gradually boosted with high intensity for 2 h (Supplementary Fig. 20). Additionally, epigallocatechin gallate (EGCG) was utilized for dose-dependent inhibition of TERT mRNA expression. When incubated with HeLa cells at a concentration of EGCG of 250 μg/mL, no fluorescence was observed, implying an inhibition on TERT mRNA expression in HeLa cells and the excellent biocompatibility of PyTPA-DNA probe (Supplementary Fig. 21). Silole-R and TP were used to monitor the cellular fluorescence responses with AZT or EGCG-treatment (Supplementary Figs 22 and 23). The fluorescence of Silole-R was lighted up when coexisting with HeLa cells without any treatment. Furthermore, the intracellular fluorescence results demonstrated that the bioprobes could successfully monitor the intracellular TERT mRNA level and telomerase activity when coexisting with HeLa cells (Supplementary Fig. 24). As such, because of the fluorescence switch-on visualization of TERT mRNA and telomerase activity in cells, imaging capabilities of high accuracy, sensitivity, and positive relationship between fluorescence intensity and TERT mRNA or telomerase activity were achieved by our system.

Fluorescence imaging of the expression of TERT mRNA (Supplementary Fig. 25) and telomerase activity (Supplementary Fig. 26) were carried out in different synchronized HeLa cells. After incubating a cell with two probes, an enhancement of the cellular fluorescence intensity was observed upon most cells; both red fluorescence and blue fluorescence were gradually increased in G1/S and S phase (Fig. 2G), potentially owing to increasing activity of telomerase over cell division from G0/G1 to S phase. Furthermore, the average fluorescence drastically reduced in G2/M phase cells, which was almost half of the initial fluorescence. The intracellular fluorescence intensities of PyTPA-DNA corrected against background signal in the cell cycle of G0/G1 phase (6.8 a.u.), S phase (10.1 a.u.) and G2/M phase (3.7 a.u.) are shown in Fig. 2H. The fluorescence
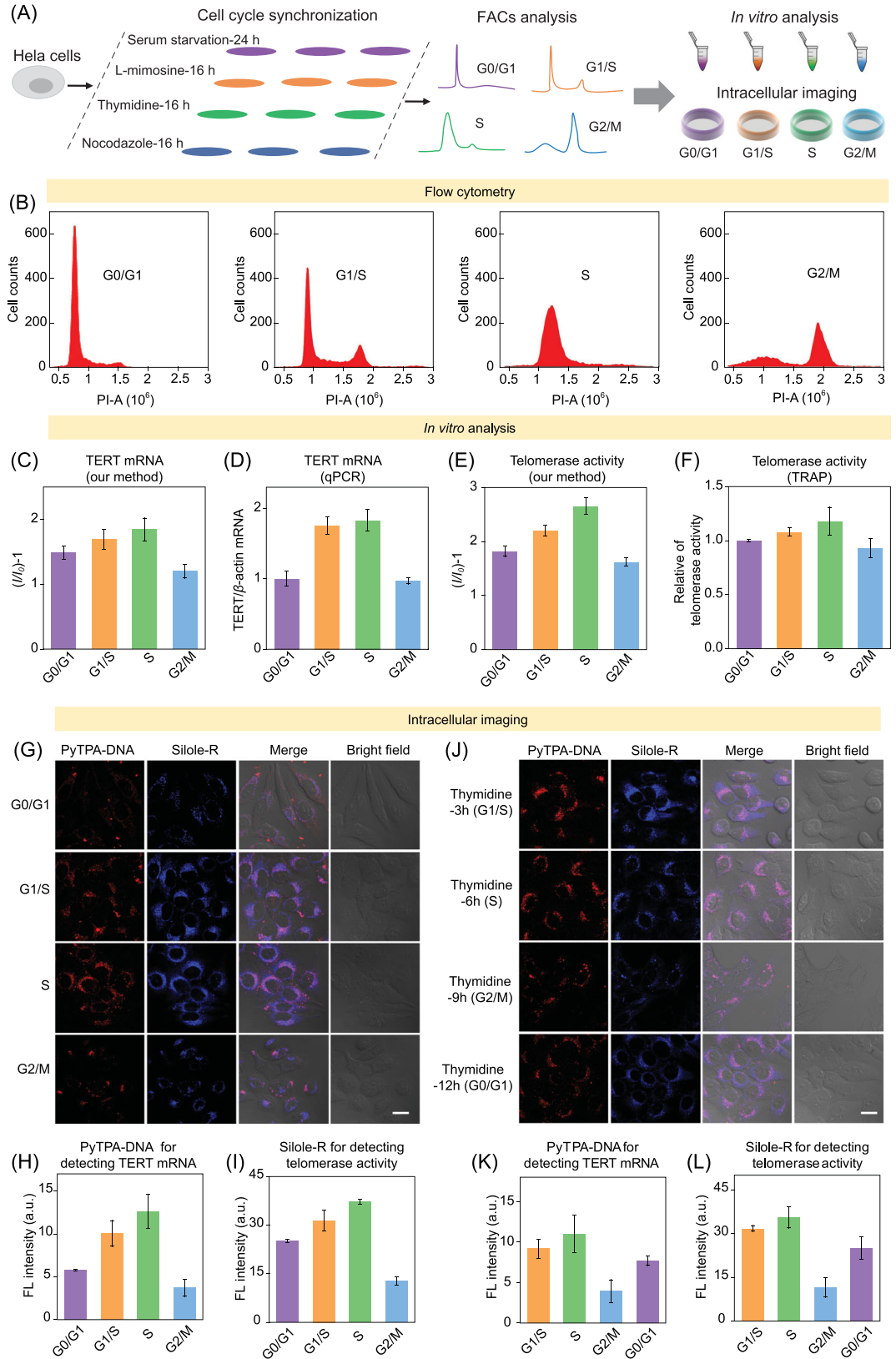
(A) Cell cycle synchronization — FACs analysis — *In vitro* analysis

(B) Flow cytometry

In vitro analysis

(C) TERT mRNA (our method)
(D) TERT mRNA (qPCR)
(E) Telomerase activity (our method)
(F) Telomerase activity (TRAP)

Intracellular imaging

(G) PyTPA-DNA, Silole-R, Merge, Bright field
(J) PyTPA-DNA, Silole-R, Merge, Bright field

(H) PyTPA-DNA for detecting TERT mRNA
(I) Silole-R for detecting telomerase activity
(K) PyTPA-DNA for detecting TERT mRNA
(L) Silole-R for detecting telomerase activity

Figure 2. (A) Illustration of brief experimental procedure. (B) Cells were synchronized at the phases of G0/G1, G1/S, S and G2/M. (C and D) Quantification of TERT mRNA in HeLa cells by PyTPA-DNA bioprobes (*I*, average fluorescence intensity at 650 nm of cancer cell samples; I_0, blank samples) and qPCR. (E and F) Quantification of telomerase activity in HeLa cells with Silole-R bioprobes (*I*, average fluorescence intensity at 478 nm of cancer cell samples; I_0, blank samples) and TRAP method. (G–I) Images of TERT mRNA and telomerase activity in different HeLa cells synchronized at the G0/G1, G1/S, S and G2/M phases and their corresponding fluorescence intensity. (J–L) Images of TERT mRNA and telomerase activity in different HeLa cells synchronized at the G1/S, S, G2/M and G0/G1 phases and their corresponding fluorescence intensities. All scale bars are 20 μm.

intensity of Silole-R corrected against background signal for HeLa cells resident in G0/G1, S and G2/M phase of the cell cycle accounted for 16.7 a.u., 48.5 a.u. and 32.7 a.u., respectively (Fig. 2I). To further confirm the contribution of the cell cycle to varied responses of fluorescence, cellular fluorescence was selectively analyzed when treated with thymidine, which was reported to affect cell behaviors to obtain different cell cycle [46,47]. Thus, fluorescence of HeLa cells treated with thymidine was monitored and found to demonstrate the highest value in S phase and related lower value in G2/M phase and almost the same signal in G1/S and G0/G1 stages (Fig. 2J–L). The intracellular fluorescence imaging results demonstrated that the cell cycle has dramatic effects on the localization of TERT mRNA and telomerase activity—the telomerase was specific boosted in the S phase and reduced in the G2/M phase in human cancer cells.

Cell-cycle-regulated TERT mRNA and telomerase activity in clinical tissue samples

We tested the expression level of TERT mRNA and telomerase activity in different periods of HeLa cells, human lung fibroblasts (HFL-1) cells and tissue specimens. Serum starvation at different times induced HFL-1 cells to arrest at different phases of the cell cycle (G0/G1, G1/S, S and G2/M) [48]. The expression level of TERT mRNA and active telomerase in normal cells revealed that somatic cells have almost no activation of telomerase during three phases of the cell cycle (Fig. 3A and B). The levels of TERT mRNA and active telomerase in most phases of the cell cycle (G0/G1, G1/S, S) are above normal cells according to the definition of $(I/I_0) - 1$, while cells arrested in G2/M phase exhibited almost the same level of HFL-1 as normal cells. Those results remind us to take cell cycle into consideration when we use TERT mRNA and telomerase activity as the early diagnosis of tumor lesion.

To verify the application value of our proposed imaging strategy in clinical samples, both PyTPA-DNA and Silole-R bioprobes were employed to detect the level of TERT mRNA and active telomerase in tissue specimens from clinical patients, such as malignant tumor, ovarian cyst, benign tumor and normal samples. The detecting results of TERT mRNA and telomerase activity showed signal increase ratios of 2/2 (100%) for cancer tissues and 1/2 (50%) for ovarian cysts from normal tissues (Fig. 4A and B) according to the definition of fluorescence intensity ratios between the normal specimens.

We further examined the expressions of TERT mRNA and active telomerase in tissues by using our proposed imaging strategy. As shown in Fig. 4C–E, Confocal Laser Scanning Microscope (CLSM) images showed that two cancer tissues displayed obvious red and blue fluorescence intensity when incubating with PyTPA-DNA and Silole-R, respectively. The tissue of cervical cancer and ovarian cancer was mainly located in the stage of cell proliferation, which was verified by immuno-histochemical (IHC) staining for Ki67 and Proliferating Cell Nuclear Antigen (PCNA) (Fig. 4F). Moreover, fluorescence intensity of ovarian cysts was much higher than that of normal tissues. Both normal tissues exhibited almost non-fluorescence in the presence of PyTPA-DNA and Silole-R. On the other hand, the tissues were consistent with hematoxylin-eosin (H&E) staining (Supplementary Fig. 27).
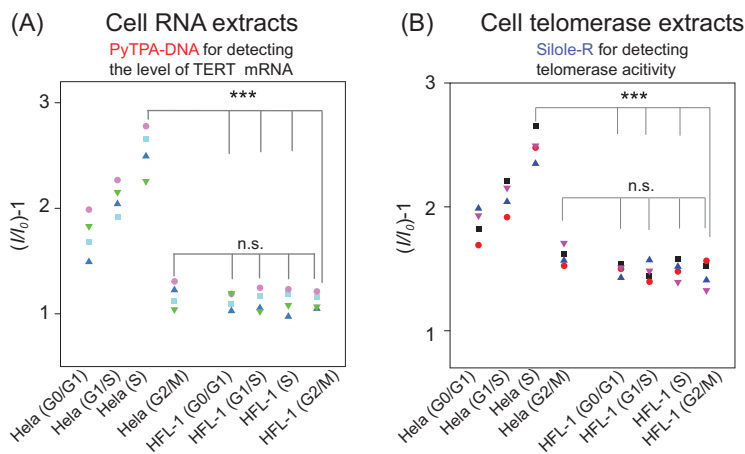

Figure 3. (A) Fluorescence response I/I_0 of TERT mRNA in different phases of HeLa cells and normal cells (*I*, average fluorescence intensity at 650 nm of cancer cell samples; I_0, blank samples). (B) Fluorescence response I/I_0 of telomerase activity in different phases of HeLa cells and normal cells (*I*, average fluorescence intensity at 478 nm of cancer cell samples; I_0, blank samples).
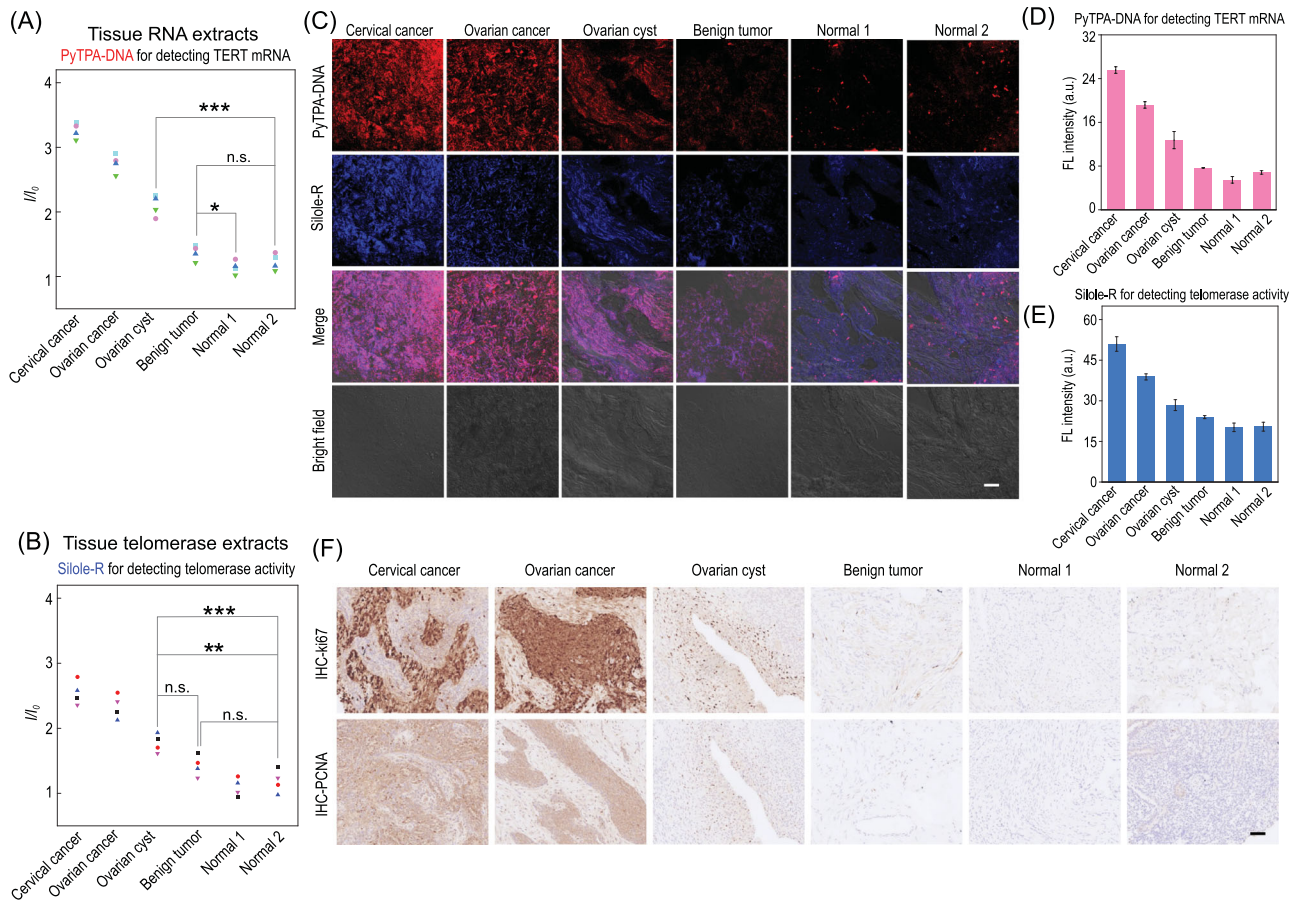
Figure 4. (A and B) Fluorescence response I/I_0 of TERT mRNA and telomerase activity in various tissue specimens. (C–E) Images of the expression of TERT mRNA, telomerase activity in different tissue specimens and their corresponding fluorescence intensities. (F) The IHC staining images of Ki67 and PCNA in tissue specimens. Scale bar, 20 μm.
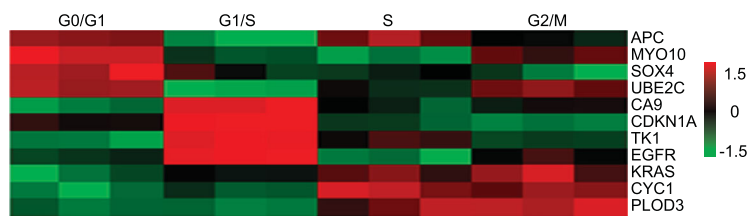

Figure 5. The expression of tumor markers during different phases of the cell cycle.

Other biomarkers also vary as the cell cycle progresses

In order to acquire a map of transcriptome information during different phases of the cell cycle, RNA sequencing was performed by using dividing cells synchronization. First, a list of known cell-cycle-regulated genes was selected [49,50] and found to have peak expression in each of our groups (Supplementary Fig. 28). Then, the level of TERT gene expression in each cell cycle was investigated (Supplementary Fig. 29) and it was consistent with the above-mentioned results. Next, great interest is aroused in analyzing the expression of genes and corresponding pathways during different phases of the cell cycle (Supplementary Figs 30–35), which is an important research area related to disease screening. Moreover, some biomarkers for various cancer detection were casually chosen to determine their expression level during different phases of the cell cycle, which suggested that tumor biomarkers were highly diversified. As shown in Fig. 5, the parameters of CA9, CDKN1A, TK1 and EGFR were significantly elevated in G1/S stage. However, the activities of KRAS, CYC1 and PLOD3 were remarkably weakened in G0/G1 and G1/S phases. Based on evaluation, these results indicated that different tumor markers were highly diversified and varied in the functions of different cell cycles.

CONCLUSION

In summary, we have constructed a highly sensitive system for imaging the cellular expression of TERT mRNA and telomerase activity during different phases of the cell cycle based on AIEgens. We found that TERT mRNA and telomerase activity

varied during the cell cycle and were able to affect the accuracy of cancer identification. The fluorescence intensities of cancer cells arrested at the phases G1/S and S were increased. In contrast, the cancer cells arrested at the phase G2/M and normal cells showed a negligible fluorescence intensity, which suggested a significant role of the cell cycle progression in regulation of telomerase activation. Herein, the cell cycle accounted for the sensitivity and efficiency of diagnosis in the field of telomerase identification.

It is worth noting that the cell cycle had a major role in cellular processes and had the ability to modulate various biomarkers. Some tumor biomarkers varied as the cell cycle progressed, such as CA9, TK1 and EGFR, which were more abundantly expressed at early S stage. Hence, our AIEgens bioprobes provided potent tools of differentiation of TERT mRNA and telomerase activity in the cell cycle and an important guidance tool for the development of probes for cell-cycle-dependent detection.

METHODS

Telomerase activity detection by Silole-R bioprobe

Telomerase extracts from different numbers of HeLa cells and HFL-1 cells were first diluted in lysis buffer and stored in the $-80°C$ refrigerator. Telomerase extracts and 7.8 μM Silole-R with dNTPs, TP and RNase inhibitor were incubated at $37°C$ for 1 h, then transferred to $94°C$ for 5 min to end the extension. Finally, the fluorescence emission spectra were measured in the range from 400 to 700 nm ($\lambda_{ex}=$ 360 nm).

TERT mRNA detection by PyTPA-DNA

The 50 μL solution consisted of PyTPA-DNA (10 μmol/L), Exo III (1 U/μL), Helps 1-2 (4 μmol/L), dNTPs (200 μmol/L), recombinant RNase inhibitor (0.8 U/μL) and varying concentrations of RNA extracts. After incubation at $37°C$ for 1 h, the reaction mixture was transferred to $95°C$ for 5 min to stop the reaction.

Electrophoresis experiment

PAGE (12%) in 1 × TBE was used to test different samples (with 1 × loading buffer) at 100 V, $24°C$. After separation, the gel was stained with Gel Red and photographed under a UV lamp.

Cellular imaging of TERT mRNA and telomerase activity

HeLa cells were seeded in a 20 mm confocal dish for 24–48 h. For imaging of TERT mRNA,

PyTPA-DNA (5 μM) and 0.5 U/μL Exo III were transfected into cells by using lipofectamine 2000 (4 μL) in Opti-MEM for 1–3 h. Subsequently, transfection mixtures were removed from cells by using PBS buffer. For imaging of telomerase activity, the 3.6 μM TP was transfected using 3 μL of lipofectamine-2000 in Opti-MEM at $37°C$ for 1 h. Subsequently, 5.0 μM Silole-R was added into the medium for 30 min. Before the imaging observation, cells had to be washed three times by using PBS buffer.

Clinical sample imaging of TERT mRNA

The clinical tissue samples were incubated with the above cellular TERT mRNA and telomerase activity imaging mixture for 1 h. Then, corresponding samples were washed with PBS buffer three times under a Zeiss LSM 880 confocal laser scanning microscope.

SUPPLEMENTARY DATA

Supplementary data are available at *NSR* online.

AUTHOR CONTRIBUTIONS

X.W., F.X. and X.D.L. conceived the project and designed the experiments. J.W., X.D.L. and F.X. supervised the research. X.W. and D.J. performed the experiments and analyzed the data. X.W., J.W., J.D., X.D.L., B.C., Z.C., F.W. and S.X.W. helped to analyze the data and provided valuable advice. X.W., J.W., X.D.L. and F.X. co-wrote the manuscript.

Conflict of interest statement. None declared.

REFERENCES

1. Kyo S, Takakura M and Inoue M. Telomerase activity in cancer as a diagnostic and therapeutic target. *Histol Histopathol* 2000; **15**: 813–24.

2. Harley CB, Kim NW and Prowse KR *et al.* Telomerase, cell immortality and cancer. *Cold Spring Harb Symp Quant Biol* 1994; **59**: 307–15.

3. Kim NW, Piatyszek MA and Prowse KR *et al.* Specific association of human telomerase activity with immortal cells and cancer. *Science* 1994; **266**: 2011–5.

4. Yuan X, Larsson C and Xu D. Mechanisms underlying the activation of TERT transcription and telomerase activity in human cancer: old actors and new players. *Oncogene* 2019; **38**: 6172–83.

5. Program T, Street C and Haven N *et al.* Cell cycle-dependent modulation of telomerase activity in tumor cells. *Proc Natl Acad Sci USA* 1996; **93**: 6091–5.

6. Kruk PA, DK O and Bohr VA. Telomerase activity is elevated in early S phase in hamster cells. *Biochem Biophys Res Commun* 1997; **233**: 717–22.

7. Weinrich SL, Pruzan R and Ma L *et al.* Reconstitution of human telomerase with the template RNA component hTR and the catalytic protein subunit hTRT. *Nat Genet* 1997; **17**: 498–502.

8. Meyerson M, Counter CM and Eaton EN *et al.* hEST2, the putative human telomerase catalytic subunit gene, is up-regulated in tumor cells and during immortalization. *Cell* 1997; **90**: 785–95.

9. Hahn WC and Meyerson M. Telomerase activation, cellular immortalization and cancer. *Ann Med* 2001; **33**: 123–9.

10. McEachern MJ, Krauskopf A and Blackburn EH. Telomerase and their control. *Annu Rev Genet* 2000; **34**: 331–58.

11. Wyatt HDM, Tsang AR and Lobb DA *et al.* Human telomerase reverse transcriptase (hTERT) Q169 is essential for telomerase function *in vitro* and *in vivo*. *PLoS One* 2009; **4**: e7176.

12. Kolquist KA, Ellisen LW and Counter CM *et al.* Expression of TERT in early premalignant lesions and a subset of cells in normal tissues. *Nat Genet* 1998; **19**: 182–6.

13. Lopez R, Wang R and Seelig G. A molecular multi-gene classifier for disease diagnostics. *Nat Chem* 2018; **10**: 746–54.

14. Sun H, Hong M and Yang Q *et al.* Visualizing the down-regulation of hTERT mRNA expression using gold-nanoflare probes and verifying the correlation with cancer cell apoptosis. *Analyst* 2019; **144**: 2994–3004.

15. Huang DS, Wang Z and He XJ *et al.* Recurrent TERT promoter mutations identified in a large-scale study of multiple tumour types are associated with increased TERT expression and telomerase activation. *Eur J Cancer* 2015; **51**: 969–76.

16. El-Mazny A, Sayed M and Sharaf S. Human telomerase reverse transcriptase messenger RNA (TERT mRNA) as a tumour marker for early detection of hepatocellular carcinoma. *Arab J Gastroenterol* 2014; **15**: 68–71.

17. Kim NW, Wu F and Corporation G *et al.* Advances in quantification and characterization of telomerase activity by the telomeric repeat amplification protocol (TRAP). *Nucleic Acids Res* 1997; **25**: 2595–7.

18. Herbert B, Hochreiter AE and Wright WE *et al.* Nonradioactive detection of telomerase activity using the telomeric repeat amplification protocol. *Nat Protoc* 2006; **1**: 1583–90.

19. Yang B, Shi L and Lei J *et al.* Advances in optical assays for detecting telomerase activity. *Luminescence* 2019; **34**: 136–52.

20. Wang J, Wu L and Ren J *et al.* Visualizing human telomerase activity with primer-modified Au nanoparticles. *Small* 2012; **8**: 259–64.

21. Xu X, Wei M and Liu Y *et al.* A simple, fast, label-free colorimetric method for detection of telomerase activity in urine by using hemin-graphene conjugates. *Biosens Bioelectron* 2017; **87**: 600–6.

22. Wen J, Yang X and Wang K *et al.* Telomerase catalyzed fluorescent probes for sensitive protein profiling based on one-dimensional microfluidic beads array. *Biosens Bioelectron* 2008; **23**: 1788–92.

23. Ling P, Lei J and Ju H. Nanoscaled porphyrinic metal-organic frameworks for electrochemical detection of telomerase activity via telomerase triggered conformation switch. *Anal Chem* 2016; **88**: 10680–6.

24. Wu J, Hu Q and Chen Q *et al.* Modular DNA-incorporated aggregation-induced emission probe for sensitive detection and imaging of DNA methyltransferase. *ACS Appl Bio Mater* 2020; **3**: 9002–11.

25. Dai J, Chen Y and Wu J *et al.* Modular peptide probe for pre/intra/postoperative therapeutic to reduce recurrence in ovarian cancer. *ACS Nano* 2020; **24**: 14698–714.

26. Wang J, Wang Y and Hu X *et al.* Dual-aptamer-conjugated molecular modulator for detecting bioactive metal ions and inhibiting metal-mediated protein aggregation. *Anal Chem* 2019; **91**: 823–9.

27. Huang J, Zhu L and Ju H *et al.* Telomerase triggered DNA walker with a super-hairpin structure for human telomerase activity sensing. *Anal Chem* 2019; **91**: 6981–5.

28. Qian R, Ding L and Yan L *et al.* Smart vesicle kit for *in situ* monitoring of intracellular telomerase activity using a telomerase-responsive probe. *Anal Chem* 2014; **86**: 8642–8.

29. Qian R, Ding L and Ju H. Switchable fluorescent imaging of intracellular telomerase activity using telomerase-responsive mesoporous silica nanoparticle. *J Am Chem Soc* 2013; **135**: 13282–5.

30. Fan H, Bai H and Liu Q *et al.* Monitoring telomerase activity in living cells with high sensitivity using cascade amplification reaction-based nanoprobe. *Anal Chem* 2019; **91**: 13143–51.

31. Feng Q, Zhu M and Zhang T *et al.* A novel DNA tetrahedron-hairpin probe for *in situ* "off-on" fluorescence imaging of intracellular telomerase activity. *Analyst* 2016; **141**: 2474–80.

32. Lou X, Zhuang Y and Zuo X *et al.* Real-time, quantitative lighting-up detection of telomerase in urines of bladder cancer patients by AIEgens. *Anal Chem* 2015; **87**: 6822–7.

33. Zhuang Y, Huang F and Xu Q *et al.* Facile, fast-responsive, and photostable imaging of telomerase activity in living cells with a fluorescence turn-on manner. *Anal Chem* 2016; **88**: 3289–94.

34. Min X, Xia L and Zhuang Y *et al.* An AIEgens and exonuclease III aided quadratic amplification assay for detecting and cellular imaging of telomerase activity. *Sci Bull* 2017; **62**: 997–1003.

35. Cheng Y, Dai J and Sun C *et al.* An intracellular H_2O_2-responsive AIEgen for the peroxidase-mediated selective imaging and inhibition of inflammatory cells. *Angew Chem Int Ed* 2018; **57**: 3123–7.

36. Cheng Y, Sun C and Liu R *et al.* A multifunctional peptide-conjugated AIEgen for efficient and sequential targeted gene delivery into the nucleus. *Angew Chem Int Ed* 2019; **58**: 5049–53.

37. Xia F, Wu J and Wu X *et al.* Modular design of peptide- or DNA-modified AIEgen probes for biosensing applications. *Acc Chem Res* 2019; **52**: 3064–74.

38. Yang H, Li M and Li C *et al.* Unraveling dual aggregation-induced emission behavior in steric-hindrance photochromic system for super resolution imaging. *Angew Chem Int Ed* 2020; **59**: 8560–70.

39. Coffman JA. Cell cycle development. *Dev Cell* 2004; **6**: 321–7.

40. Nishitani H and Lygerou Z. Control of DNA replication licensing in a cell cycle. *Genes Cells* 2002; **7**: 523–34.

41. Kar S. Unraveling cell-cycle dynamics in cancer. *Cell Syst* 2016; **2**: 8–10.

42. Zhao YM, Li JY and Lan JP *et al.* Cell cycle dependent telomere regulation by telomerase in human bone marrow mesenchymal stem cells. *Biochem Biophys Res Commun* 2008; **369**: 1114–9.

43. Tomlinson RL, Ziegler TD and Supakorndej T *et al.* Cell cycle-regulated trafficking of human telomerase to telomeres. *Mol Biol Cell* 2006; **17**: 955–65.

44. Nielsen NH, Nilsson N and Emdin S *et al.* Telomerase activity is associated with cell cycle deregulation in human. *Cancer Res* 1997; **57**: 549–54.

45. Yang J, Dai J and Wang Q *et al.* Tumor-triggered disassembly of a multiple-agent-therapy probe for efficient cellular internalization. *Angew Chem Int Ed* 2020; **59**: 20405–10.

46. Tong J, Sun D and Yang C *et al.* Serum starvation and thymidine double blocking achieved efficient cell cycle synchronization and altered the expression of p27, p53, bcl-2 in canine breast cancer cells. *Res Vet Sci* 2016; **105**: 10–4.

47. Thomas DB and Lingwood CA. A model of cell cycle control: effects of thymidine on synchronous cell cultures. *Cell* 1975; **5**: 37–44.

48. Chen M, Huang J and Yang X *et al.* Serum starvation induced cell cycle synchronization facilitates human somatic cells reprogramming. *PLoS One* 2012; **7**: e28203.

49. Bar-Joseph Z, Siegfried Z and Brandeis M *et al.* Genome-wide transcriptional analysis of the human cell cycle identifies genes differentially regulated in normal and cancer cells. *Proc Natl Acad Sci USA* 2008; **105**: 955–60.

50. Whitfield ML, Sherlock G and Saldanha AJ *et al.* Identification of genes periodically expressed in the human cell cycle and their expression in tumors. *Mol Biol Cell* 2002; **13**: 1977–2000.